NANO LETTERS

LETTER

pubs.acs.org/NanoLett

Electronic−Mechanical Coupling in Graphene from in situ Nanoindentation Experiments and Multiscale Atomistic Simulations

Mingyuan Huang,[*,†] Tod A. Pascal,[‡,§] Hyungjun Kim,[‡,§] William A. Goddard, III,[‡,§] and Julia R. Greer[†]

[†]Division of Engineering and Applied Science, California Institute of Technology, 1200 East California Boulevard, MC 309-81, Pasadena, California 91125-8100, United States

[‡]Center for Materials Simulations and Design, Graduate School of EEWS, Korea Advanced Institute of Science and Technology, Daejeon, Korea

[§]Materials and Process Simulation Center, California Institute of Technology, 1200 East California Boulevard, MC 309-81, Pasadena, California 91125-8100, United States

S *Supporting Information*

ABSTRACT:

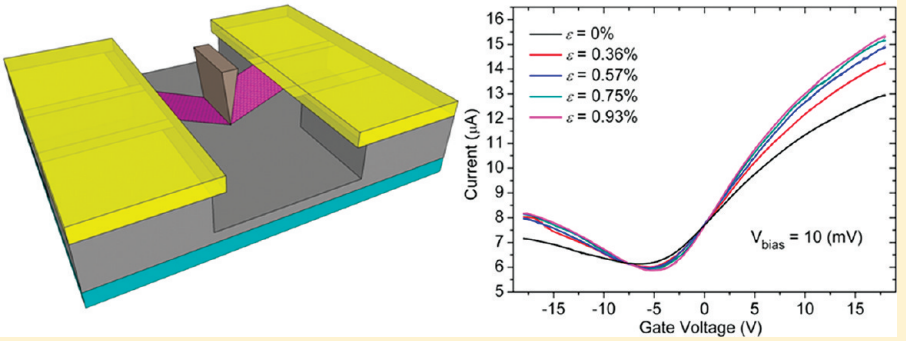

We present the in situ nanoindentation experiments performed on suspended graphene devices to introduce homogeneous tensile strain, while simultaneously carrying out electrical measurements. We find that the electrical resistance shows only a marginal change even under severe strain, and the electronic transport measurement confirms that there is no band gap opening for graphene under moderate uniform strain, which is consistent with our results from the first-principles informed molecular dynamics simulation.

KEYWORDS: Graphene, nanoindentation, strain, electronic properties

Graphene, a truly two-dimensional gapless semiconductor,[1,2] recently deemed strongest material ever measured, can sustain very high, up to 25%, in-plane tensile elastic strains.[3] Straining graphene to such a significant elongation is likely to shift its electronic band structure and elicit intriguing electronic properties, resulting in notable electrical−mechanical coupling. Several recent theoretical-only studies on strained graphene predict that strain can shift the Dirac cones, reduce the Fermi velocity, introduce a pseudomagnetic field, and be used to engineer the electronic structure.[4−10] Moreover, theory also suggests that uniaxial strains below a very high value of ∼23% would not be capable of opening a band gap in graphene,[5] which may be crucial for the utilization of this material in future electronic devices. On the experimental side, optical measurements revealed that strain induces a disruption of graphene's symmetry and a shift of the Dirac cone,[11−13] while scanning tunneling microscopy (STM) studies conveyed the presence of a pseudomagnetic field in highly strained graphene nanobubble systems.[14] However, no direct experiments on electrical measurements of strained graphene have yet been reported. Here, we present the results of in situ investigation of electrical−mechanical coupling in graphene-based devices.

The suspended graphene devices were fabricated by a process analogous to that described in previous reports[15,16] and outlined in detail in the Supporting Information. To ensure strain uniformity during nanoindentation tests, graphene flakes were patterned into graphene ribbons with widths between 1.5 and 4 μm and lengths between 0.8 and 1.2 μm. This type of geometry ensured that the ribbon was sufficiently long to carry out the experiment yet not too long as to render the mechanical load below the detection limit of our system. Figure 1a shows a scanning electron microscopy (SEM) image of multiple suspended devices made from a single graphene flake, and Figure 1b shows a zoomed-in SEM image of a representative device. Figure 1c shows a schematic of nanoindentation into a suspended graphene ribbon device. The black curve in Figure 1d shows a typical electronic transport result of a suspended graphene device.

The nanoindentation experiments on graphene ribbons were carried out in a custom-built instrument, SEMentor, composed of a field-emission gun SEM (Quanta200 FEG, FEI) and a

Received: December 3, 2010
Revised: January 25, 2011
Published: February 10, 2011

nanomechanical module similar to a nanoindenter, as shown in

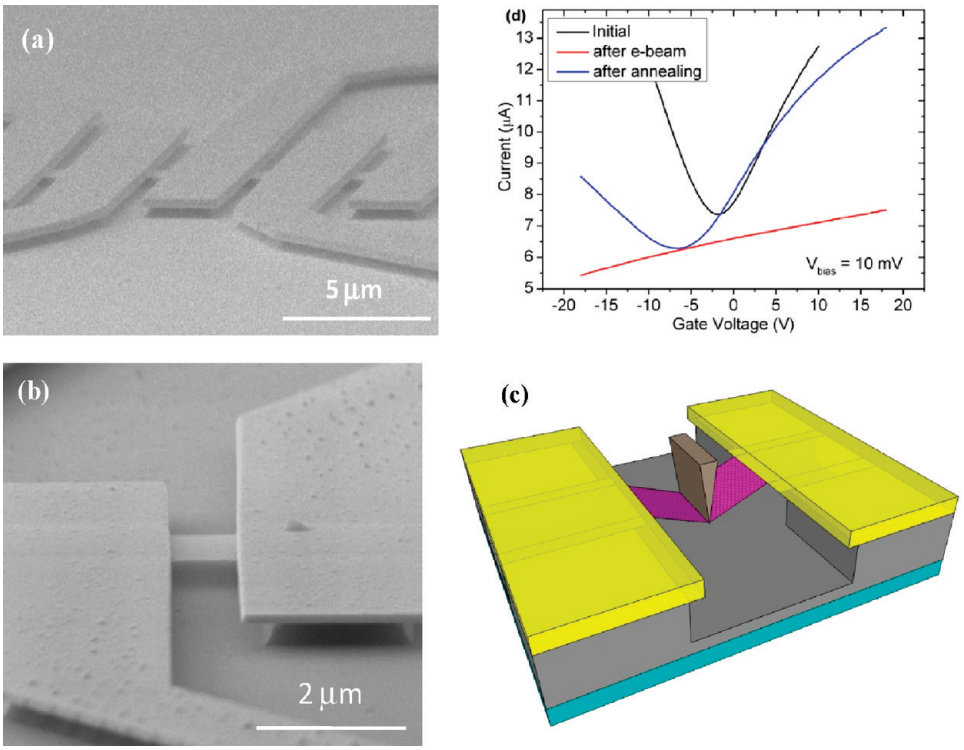

Figure 1. Fabrication and electrical characterization of suspended graphene. (a) SEM image of four suspended graphene devices made from a single flake. (b) A zoomed-in SEM image of a single suspended graphene device. (c) Schematic of a suspended graphene device with a wedge tip indenting the graphene ribbon. Because the BOE can diffuse along the graphene, the oxide beneath the graphene was etched away. (d) Electronic transport measurement of a graphene device before exposing to e-beam (black curve), after a short exposure to the e-beam (red curve), and after electrical annealing (blue curve).

Figure 2a. The wedge indentation tip, shown in the lower left inset, was fabricated by using focused ion beam (FIB) from a commercially available diamond Berkovich indenter tip. By applying a load at the center of the ribbon, the wedge tip introduces a uniform tensile strain within the graphene ribbon; with the load and displacement, as well as contact stiffness continuously measured throughout the experiment. Figure 2b shows typical load versus displacement and contact stiffness versus displacement data obtained by SEMentor. The in situ capability of SEMentor ensures a proper alignment between the indenter tip and the ribbons and provides visualization of the entire indentation process. Panels c−h of Figure 2 show a consecutive time series of video images obtained during a graphene indentation experiment (see Supporting Information). A few key observations can be made based on these images: (i) the graphene ribbon was clearly stretched (Figure 2d−g); (ii) the electrodes serving as supports for the suspended graphene slightly bent (Figure 2e,f), implying that they cannot be assumed to be perfectly rigid; (iii) the graphene appeared to adhere to the indenter tip upon unloading (Figure 2g); and (iv) the ribbon was fully recovered after the indentation, strongly suggesting the lack of slipping between the graphene and the electrodes.

Electron beam irradiation has been shown to induce defects into the graphene lattice, causing serious degradation of its electrical properties.[17−20] Indeed, our electrical measurements taken with the e-beam turned on resulted in a dramatic increase in resistance and nontrivial n-doping. Further, the e-beam induced the deposition of amorphous carbon on the sample surfaces when imaged for a long time. To eliminate these adverse e-beam irradiation-induced effects, we used a low-energy e-beam (5 kV, 50 pA) to image our samples and minimized exposure time. Further, prior to mechanical−electrical testing, we electrically annealed the samples to drive out the impurities, resulting in nearly full resistance recovery, as shown in Figure 1d. To separate the e-beam irradiation and strain-induced effects, the indenter wedge tip was first aligned at ∼200 nm above the center of graphene ribbon in the SEM, and the e-beam was then blanked. The ensuing electrical annealing and the nanoindentation experiments were performed "blindly", i.e., with no e-beam exposure following the annealing step.

Figure 2b shows a typical load and contact stiffness (inset) versus vertical displacement of the ribbon's center. The kinks in the load−displacement curve indicate that there was some adhesion between the indenter tip and graphene. This is not surprising as this type of adhesion has been previously observed in suspended carbon nanotube devices.[21] After the initial contact, the load first becomes negative but gradually increases to positive. The zero load point, which corresponds to a minimum in the contact stiffness curve, is then defined as the zero displacement point. The intentional ∼40 s long constant load holds, numerically labeled in Figure 2b, are incorporated in order to allow sufficient time to perform electrical measurements at each strain level. The maximum attained tensile strains in this type of experiment are expected to be ∼2−3%, well within the elastic-only regime.[3] The observed hysteresis in the load−displacement curve (Figure 2b) is due to the thermal drift and damping, rather than to a deviation from elasticity, as has been

dx.doi.org/10.1021/nl104227t |*Nano Lett.* 2011, 11, 1241–1246

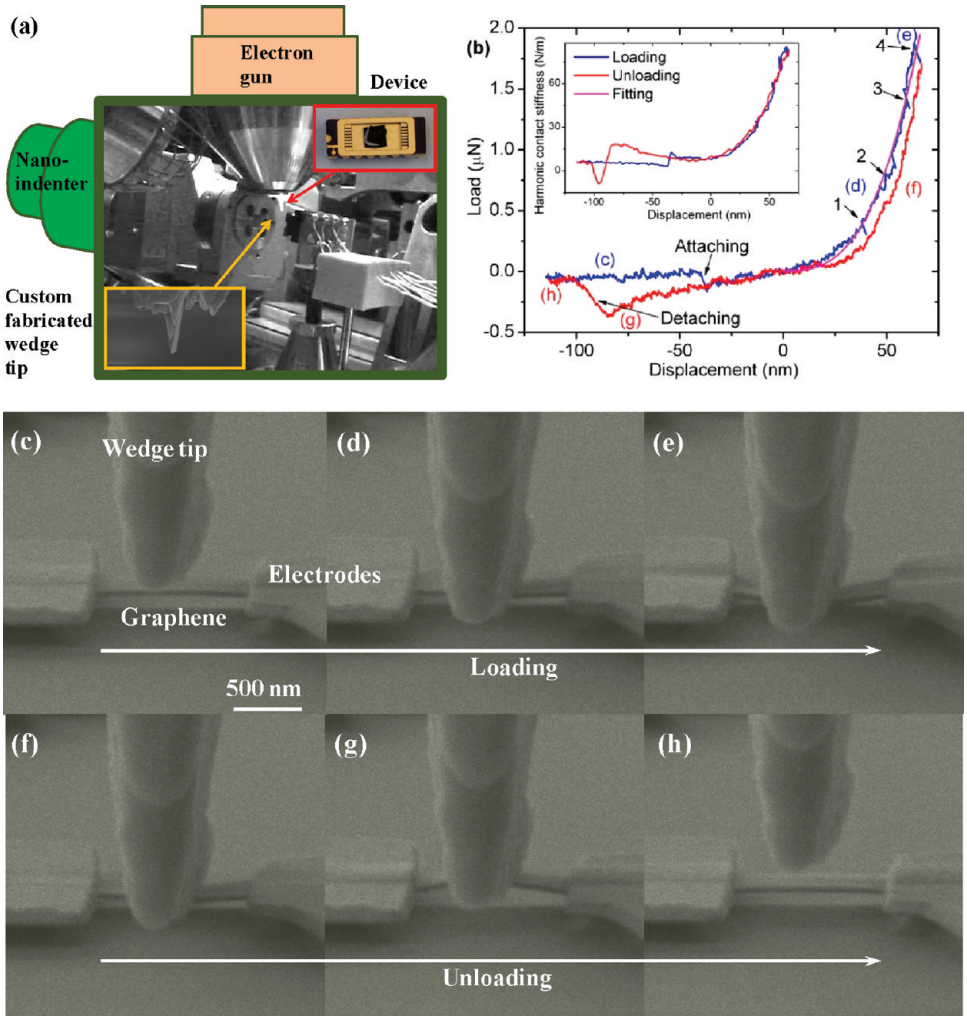

Figure 2. Experimental setup and mechanical testing results. (a) The in situ mechanical testing setup, SEMentor, is comprised of a field-emission SEM (Quanta200 FEG, FEI) and the DCM module of Agilent nanoindenter.[25,26] A custom fabricated wedge tip (inset in bottom left) and the wire-bonded device (inset in top right) are shown in the middle picture. The wires from the sample holder are connected to a Keithley source meter to perform the electrical measurements. (b) A typical load−displacement curve obtained from nanoindentation shows hysteresis due to thermal drift. The attaching and detaching of the indenter tip from graphene ribbons show a jump in the load due to the adhesion. The numerically labeled constant-load holds are used to perform the electrical measurements. The inset shows the harmonic contact stiffness vs displacement with nearly identical curves during loading and unloading. (c−h) A progressive time series of images taken from a single video taken during nanoindentation.

observed previously on suspended thin film metallic samples.[22] The 100% reversibility of the stiffness-displacement data indicates that the mechanical deformation is indeed elastic and that there was no slippage between the graphene and the electrodes.

According to a suspended bridge model developed by Herbert et al.,[22] the elastic deflection h of the center point in response to a line load P across the center of the graphene ribbon can be expressed as

$$P = \frac{8wE^{2D}}{l^3} h^3 + \frac{8w\sigma^{2D}}{l} h \qquad (1)$$

where w and l are the width and the length of the graphene ribbon, E^{2D} is the two-dimensional Young's modulus, and σ^{2D} is the residual tension in the as-fabricated ribbon. While this equation was found to describe the deflection of suspended metallic films well, the model's fundamental assumption is that the effects of the bending moments are negligible, so that only stretching is dominating the deformation. We find this assumption to be valid for our graphene analysis since its thickness is 4 orders of magnitude smaller than its length. Another assumption of this model is that the support electrodes are infinitely stiff. However, as can be clearly seen in Figure 2e, the electrodes bent during the deformation. To address this issue, we used finite element method (ABAQUS) to simulate the bending of the electrodes and to calculate this additional bending stiffness (see Figure S1, Supporting Information). The additional displacement due to this bending is then subtracted from the overall deflection measured by the instrument to obtain the true load versus displacement relationship for the graphene ribbon, as shown in Figure 2b. The purple line here is the fit of the loading data, based on eq 1, with E^{2D} and σ^{2D} extrapolated from the fit and with the data collected from 10 high-quality samples. The mean extrapolated Young's modulus is $E^{2D} = 335 \pm 20$ N/m, a value very close to that reported in other works.[3] This value corresponds to Young's modulus of $E = 1$ TPa for bulk graphite, which also agrees well with the experimental result for the in-plane Young's modulus in graphite.[23] We find that the initial

dx.doi.org/10.1021/nl104227t |*Nano Lett.* 2011, 11, 1241–1246

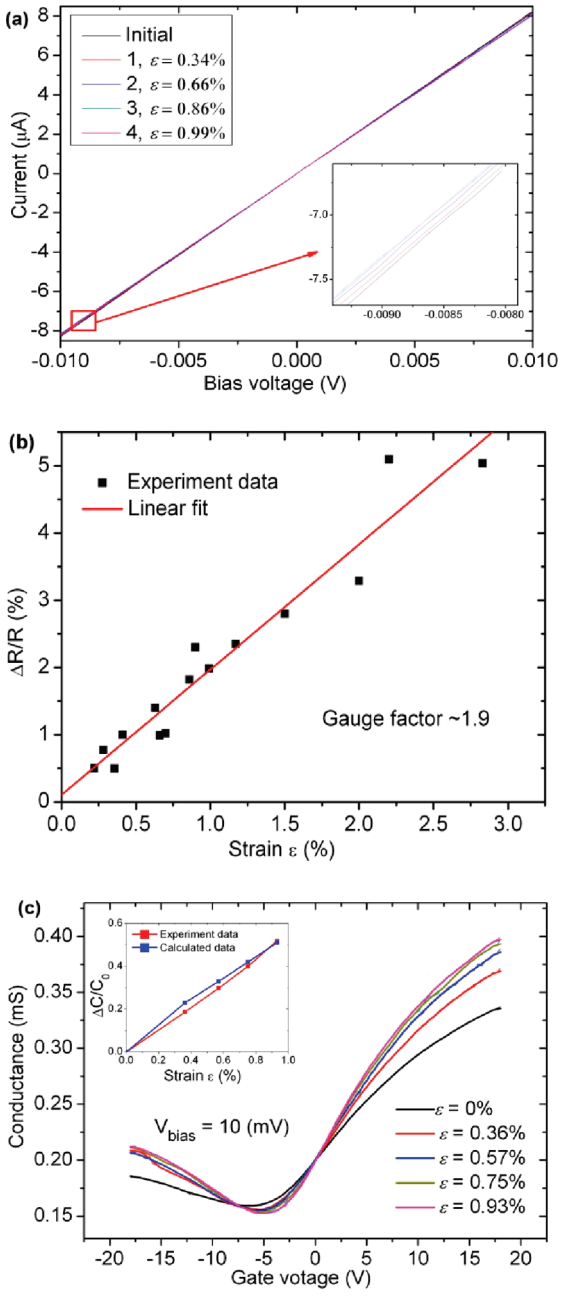

Figure 3. Electrical measurements of uniaxially strained graphene: (a) $I-V$ measurement of strained graphene; (b) relative change of resistance as function of strain; (c) electronic transport measurement of strained graphene. The inset shows the relative change of the gate capacitance from the experiment data (red) and a calculation (blue) as a function of strain.

tension σ^{2D} ranges from 0.08 to 2.4 N/m, also in reasonable agreement with previous reports.[3]

To probe the electromechanical response of graphene, we measured the conductance while indenting the graphene ribbon. Figure 3a shows the $I-V$ characteristics under low bias conditions, which were taken during the holds shown in Figure 2b. The strain ε in graphene during the holds is $\varepsilon = 2h^2/l^2$. Interestingly, no significant change in the conductance was observed up to the strains of 1%, indicating the lack of a noticeable change in the band structure of uniaxially strained graphene. On the basis of the zoomed-in $I-V$ curves, the conductance appears to decrease by ~2% with 1% strain. In this study, five different samples were measured, and the relative change in resistance, extracted by linear fitting of the $I-V$ curves, was found to be proportional to strain, as shown in Figure 3b. The gauge factor extracted from these curves was 1.9.

To further investigate the band structure of graphene under strain, the electronic transport was measured by taking the highly doped Si substrate as the back gate. Figure 3c shows the conductance as a function of gate voltage V_g for different strains. We find that our graphene ribbons can sustain up to 20 V without collapse. In addition to the load applied by the nanoindenter, the back gate can also electrostatically introduce attractive force into graphene ribbons. This force can be estimated as[15]

$$F_{ele} = \frac{\varepsilon_0 \varepsilon^2 lw}{2(d_0 + \varepsilon d_1)^2} V_g^2 \qquad (2)$$

where d_0 = 100 and d_1 = 200 nm are the thicknesses of the remaining and etched SiO_2. For the typical size of our samples, this electrostatic force is estimated to be ~1×10^{-7} N for 20 V, which is 1 order of magnitude lower than the load applied by the nanoindenter, and therefore, can be neglected during subsequent calculations.

Unlike the $I-V$ measurements, the transport in the gated graphene ribbons shows a significant change during straining, as shown in Figure 3c. On the basis of the device geometry, this change could be due to the increased capacitance, as the graphene is brought closer to the back gate. As shown in Figure 3c, the minimum conductance of graphene does not change significantly during the indentation, indicating that the electronic properties are likely unaffected. All curves in Figure 3c cross at $V_g = 0$, further corroborating that the electrical properties are unchanged. As the indenter tip pushes the graphene ribbon toward the back gate, the gate capacitance increases, thereby improving the gating efficiency, which is likely what we are observing. The relative change in the gate capacitance can be estimated by monitoring the conductance versus strain slope changes (inset in Figure 3c). This change can also be calculated from the displacement of the indenter (see Supporting Information), shown by the red points in the inset of Figure 3c. Since the calculated values are very close to the experiment data, it is likely that the observed changes in the electronic transport as a function of strain are due to the varying gate capacitance and not to an alteration in the band structure.

To improve our understanding of the mechanical deformation of graphene at the atomic level, we used extensive molecular dynamics simulations to quantify the effect of indentation on the local carbon lattice structure. Since the results of such simulations depend critically on the interaction potential and, in particular, on the accuracy of the in-plane phonon modes, we based our simulations on the QMFF-Cx force field[24] validated to reproduce the mechanical and thermodynamic properties of graphite. The force field was determined from first principles quantum mechanics (QM) without empirical parameters that would bias it toward any particular set of experimental conditions. This last point is critical, as it allows for the direct application of the force field to other graphitic materials, under various thermodynamic conditions. We test the applicability of QMFF-Cx for graphite by first calculating the mechanical properties at 0 K. We find that the Young's modulus (1092.7 GPa) and in-plane bulk compressibilities (0.023

dx.doi.org/10.1021/nl104227t |Nano Lett. 2011, 11, 1241–1246

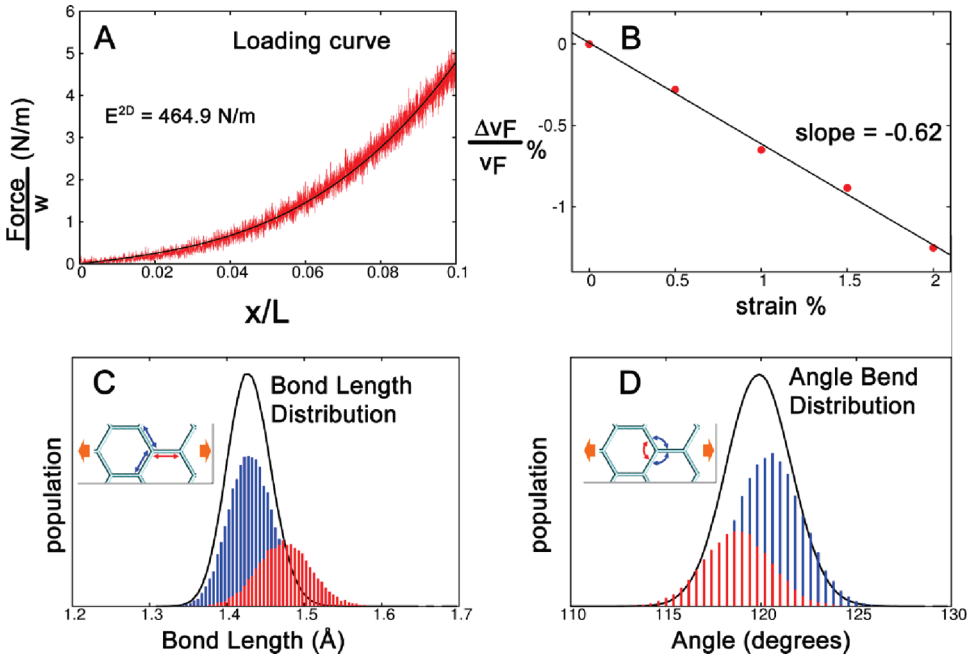

Figure 4. (a) Force loading curve as calculated by the MD simulations (red line) is fitted by eq 1 (black line). The indentation occurs along the y dimension. (b) Estimated relative change of Fermi velocity vs strain while stretching graphene. (c) Bond length distribution after full loading of the indenter (x/L = 0.1). The bond in the x dimension (perpendicular to the indenter) is stretched (1.429 Å → 1.474 Å) while the bonds along the y direction (parallel to the indenter) remain nearly constant (1.429 Å → 1.431 Å). The equilibrium bond length distributions (black line) are shown as a reference. (d) Angle bending distribution. Angles in the y direction (red) are compressed (120° → 118.7°) while the angles along the x direction (blue) are stretched (120° → 120.5°) compared to the equilibrium angle distribution (black).

1/GPa) are in good agreement with experiments (1020 ± 30 GPa and 0.026 1/GPa, respectively).

Our MD simulations indicate that the local graphene structure is relatively insensitive to the indentation at the studied strains. From the force−displacement curves (Figure 4a), we calculate Young's modulus (463.1 N/m) in good agreement with the experimental values of 335 ± 20 N/m. More importantly, we find a decoupling in the bond stretch distributions (Figure 4c) during indentations: with the bonds along the x direction (perpendicular to the indenter) stretched (1.429 Å → 1.474 Å) while the bonds along the y direction (parallel to the indenter) remain nearly constant (1.429 Å → 1.431 Å). Conversely, the angles (Figure 4d) in the y direction become smaller (120° → 118.7°), while the angles along the x direction increase (120° → 120.5°). A physical interpretation of these results suggests a Poisson's ratio υ of 0.18 (2.8% stretching along the x direction and 0.5% shrink along the y direction), which is in good agreement with the experimental value of 0.17.[23]

To investigate the effect of indentation on the electronic structure of graphene, we performed a series of density functional theory (DFT) calculations. First, we optimized the atomic positions and cell parameters of the smallest orthorhombic cell (four atoms per unit cell along the armchair direction (x direction); cell parameter along the zigzag direction (y direction) is identical to the primitive cell) to fully release the internal stresses. Then we stretched the graphene sheet along the armchair direction by increasing the x directional cell parameter by ΔL_x (up to 2% strain). Meanwhile, we decreased the y directional cell parameter by $0.17\Delta L_x$ to model the Poisson effect. We note that no band gap opening was observed under strain. By monitoring the slope of the Dirac cone from the band structure calculations, we obtained the relative change of Fermi velocity (v_F) under strain, as shown Figure 4d.

By considering the unscreened charge impurities as the dominated scattering source, which is fairly accurate due to the e-beam-induced doping and associated resistance increase, the resistivity is proportional to the inverse of square of Fermi velocity, v_F.[5] Further, the relationship between resistivity and gauge factor for graphene can be expressed as

$$\frac{\Delta R/R}{\varepsilon} = 1 + \upsilon + \frac{\Delta \rho/\rho}{\varepsilon} = 1 + \upsilon - 2\,\frac{\Delta V_F/V_F}{\varepsilon} \qquad (3)$$

On the basis of eq 3, the gauge factor of graphene can be estimated as 2.4, comparable to our measurements, 1.9.

In summary, we performed in situ nanoindentation to induce uniaxial tensile strain in suspended graphene devices and simultaneously measured the electronic transport properties. We find the Young's modulus to be ~335 N/m, consistent with previous reports and our atomistic simulation results. The electrical measurements indicate that the gauge factor of graphene is ~1.9, which is comparable to the 2.4 predicted by simulations. Our transport measurements reveal that a moderate uniaxial strain is not capable of opening a band gap in graphene and does not affect its carrier mobility. This result matches our first principle-based MD simulations, as well as other theoretical predictions. Our study shows that unlike many CMOS devices, strain, which can be easily controlled through device fabrication process, is not an effective means to alter electronic transport properties in graphene.

■ ASSOCIATED CONTENT

Supporting Information. Material contains sample fabrication details, stiffness of gold electrodes, gate capacitance, and

dx.doi.org/10.1021/nl104227t |Nano Lett. 2011, 11, 1241–1246

the details for MD and DFT simulations. This material is available free of charge via the Internet at http://pubs.acs.org.

AUTHOR INFORMATION

Corresponding Author
*E-mail: mingyuan@caltech.edu.

ACKNOWLEDGMENT

M.H. and J.R.G. gratefully acknowledge the financial support of the Nanoelectronics Research Initiative (NRI) through INDEX Center. T.A.P., H.K., and W.A.G. acknowledge support from the WCU programs through NRF of Korea funded by the MEST (R31-2008-000-10055-0). The authors also thank Changyao Chen, James Hone, and Yeojun Chun for help with sample fabrication and Zachary H. Aitken for help in finite element simulation and stimulating scientific discussion.

REFERENCES

(1) Novoselov, K. S.; Geim, A. K.; Morozov, S. V.; Jiang, D.; Katsnelson, M. I.; Grigorieva, I. V.; Dubonos, S. V.; Firsov, A. A. *Nature* **2005**, *438* (7065), 197–200.
(2) Zhang, Y. B.; Tan, Y. W.; Stormer, H. L.; Kim, P. *Nature* **2005**, *438* (7065), 201–204.
(3) Lee, C.; Wei, X.; Kysar, J. W.; Hone, J. *Science* **2008**, *321* (5587), 385–388.
(4) Pereira, V. M.; Neto, A. H. C. *Phys. Rev. Lett.* **2009**, *103* (4), No. 046801.
(5) Pereira, V. M.; Neto, A. H. C.; Peres, N. M. R. *Phys. Rev. B* **2009**, *80* (4), No. 045401.
(6) Choi, S. M.; Jhi, S. H.; Son, Y. W. *Nano Lett.* **2010**, *10* (9), 3486–3489.
(7) Cocco, G.; Cadelano, E.; Colombo, L. *Phys. Rev. B* **2010**, *81* (24), No. 241412.
(8) Guinea, F.; Katsnelson, M. I.; Geim, A. K. *Nat. Phys.* **2010**, *6* (1), 30–33.
(9) Low, T.; Guinea, F. *Nano Lett.* **2010**, *10* (9), 3551–3554.
(10) Lu, Y.; Guo, J. *Nano Res.* **2010**, *3* (3), 189–199.
(11) Huang, M. Y.; Yan, H. G.; Chen, C. Y.; Song, D. H.; Heinz, T. F.; Hone, J. *Proc. Natl. Acad. Sci. U.S.A.* **2009**, *106* (18), 7304–7308.
(12) Mohiuddin, T. M. G.; Lombardo, A.; Nair, R. R.; Bonetti, A.; Savini, G.; Jalil, R.; Bonini, N.; Basko, D. M.; Galiotis, C.; Marzari, N.; Novoselov, K. S.; Geim, A. K.; Ferrari, A. C. *Phys. Rev. B* **2009**, *79* (20), No. 205433.
(13) Huang, M. Y.; Yan, H. G.; Heinz, T. F.; Hone, J. *Nano Lett.* **2010**, *10* (10), 4074–4079.
(14) Levy, N.; Burke, S. A.; Meaker, K. L.; Panlasigui, M.; Zettl, A.; Guinea, F.; Neto, A. H. C.; Crommie, M. F. *Science* **2010**, *329* (5991), 544–547.
(15) Bolotin, K. I.; Sikes, K. J.; Jiang, Z.; Klima, M.; Fudenberg, G.; Hone, J.; Kim, P.; Stormer, H. L. *Solid State Commun.* **2008**, *146* (9−10), 351–355.
(16) Chen, C. Y.; Rosenblatt, S.; Bolotin, K. I.; Kalb, W.; Kim, P.; Kymissis, I.; Stormer, H. L.; Heinz, T. F.; Hone, J. *Nat. Nanotechnol.* **2009**, *4* (12), 861–867.
(17) Jones, J. D.; Ecton, P. A.; Mo, Y.; Perez, J. M. *Appl. Phys. Lett.* **2009**, *95* (24), No. 3272954.
(18) Teweldebrhan, D.; Balandin, A. A. *Appl. Phys. Lett.* **2009**, *95* (24), No. 3272961.
(19) Teweldebrhan, D.; Balandin, A. A. *Appl. Phys. Lett.* **2009**, *94* (1), No. 3062851.
(20) Isaac Childres; Luis A. Jauregui; Mike Foxe; Jifa Tian; Romaneh Jalilian; Igor Jovanovic; Chen, Y. P. arXiv:1008.4561, 2010.
(21) Minot, E. D.; Yaish, Y.; Sazonova, V.; Park, J. Y.; Brink, M.; McEuen, P. L. *Phys. Rev. Lett.* **2003**, *90* (15), No. 156401.
(22) Herbert, E. G.; Oliver, W. C.; Boer, M. P. d.; Pharr, G. M. *J. Mater. Res.* **2009**, *24* (9), 2974–2985.
(23) Reynolds, W. N. *Physical properties of graphite*; Elsevier Publishing Co.: Amsterdam and New York, 1968.
(24) Pascal, T. A.; Karasawa, N.; Goddard, W. A. *J. Chem. Phys.* **2010**, *133* (13), No. 134114.
(25) Greer, J. R.; Kim, J.-Y.; Burek, M. J. *J. Mater.* **2009**, *61* (12), 19–25.
(26) Kim, J. Y.; Greer, J. R. *Acta Materialia* **2009**, *57* (17), 5245–5253.